Journal of Dental Sciences 19 (2024) 502–514

Available online at www.sciencedirect.com

ScienceDirect

journal homepage: www.e-jds.com

Original Article

Use of customized 3-dimensional printed mandibular prostheses with a dental implant pressure-reducing device in mandibular body defect: A finite element study performing multiresponse surface methodology

Chun-Feng Chen [a,b,c], Wei-Chin Huang [d], Sung-Ho Liu [d], Ling-Lin Wang [a,e], Pei-Feng Liu [f], Ping-Ho Chen [a], Chun-Ming Chen [a*]

[a] School of Dentistry, College of Dental Medicine, Kaohsiung Medical University, Kaohsiung, Taiwan
[b] Department of Oral and Maxillofacial Surgery, Kaohsiung Veterans General Hospital, Kaohsiung, Taiwan
[c] Dental Laboratory Technology, Shu Zen College of Medicine & Management, Kaohsiung, Taiwan
[d] Laser and Additive Manufacturing Technology Center, Industrial Technology Research Institute, Kaohsiung, Taiwan
[e] KSVGH Originals & Enterprises, Kaohsiung Veterans General Hospital, Kaohsiung, Taiwan
[f] Department of Biomedical Science and Environmental Biology, College of Life Science, Kaohsiung Medical University, Kaohsiung, Taiwan

Received 20 August 2023; Final revision received 9 September 2023
Available online 22 September 2023

KEYWORDS
Mandibular reconstruction;
Customized mandible prothesis;
Pressure-reducing device;
Finite element

Abstract *Background/purpose:* Segmental body defects of the mandible result in the complete loss of the affected region. In our previous study, we investigated the clinical applicability of a customized mandible prosthesis (CMP) with a pressure-reducing device (PRD) in an animal study. In this study, we further incorporated dental implants into the CMP and explored the use of dental implant PRD (iPRD) designs.
Materials and methods: By employing a finite element analysis approach, we created 4 types of CMP: CMP, CMP with iPRD, CMP-PRD, and CMP-PRD with iPRD. We developed 2 parameters for the iPRD: cone length (CL) in the upper part and spring pitch (SP) in the lower part. Using

* Corresponding author. School of Dentistry, College of Dental Medicine, Kaohsiung Medical University, No 100, Shih-Chuan 1st Road, Kaohsiung 80708, Taiwan.
E-mail address: D840074@kmu.edu.tw (C.-M. Chen).

https://doi.org/10.1016/j.jds.2023.09.011

analysis;
Response surface methodology;
Human experiment

the response surface methodology (RSM), we determined the most suitable structural assignment for the iPRD.
Results: Our results indicate that CMP-PRD had the highest von Mises stress value for the entire assembly (1076.26 MPa). For retentive screws and abutments, CMP with iPRD had the highest von Mises stress value (319.97 and 452.78 MPa, respectively). CMP-PRD had the highest principal stress (131.66 MPa) in the anterior mandible. The iPRD reduced principal stress in both the anterior and posterior mandible. Using the RSM, we generated 25 groups for comparison to achieve the most favorable results for the iPRD and we might suggest the CL to 12 mm and the SP to 0.4 mm in the further clinical trials.
Conclusion: Use of the PRD and iPRD in CMP may resolve the challenges associated with CMP, thereby promoting its usage in clinical practice.

Introduction

A segmental bone defect of the mandible refers to a condition in which a specific segment of the mandible is completely lost. This condition can result from infection, mandibular osteomyelitis, tumor resection, or comminuted mandibular fracture.[1] Immediate reconstruction of the mandible is crucial to treating a large-scale mandibular defect.[1,2] Numerous methods have been used to restore the appearance and function of the mandible, including the use of reconstruction plates, microvascular fibula free flaps, iliac bone grafts, costochondral rib bone grafts, and alloplastic prostheses.[3,4] When the segmental mandible defect is too large or the composite soft tissue defect is too complicated, the application of a fibula osteocutaneous flap is a standard treatment option.[5,6] However, this method has potential disadvantages, such as donor-site morbidity, lengthy operation time, scar construction, and suboptimal cosmetic results. Typically, a mandibular body defect necessitates a fibula graft ranging from five to 7 cm.[7] If the defect is confined solely to the mandibular body, it's worth exploring alternative solutions.

Customized 3-dimensional (3D) printed mandible prostheses (CMPs) can be designed to fit the size and shape of the defect.[4,8–12] The use of computer-aided design and computer-aided manufacturing systems has enabled the incorporation of these prostheses into preoperative surgical planning and the production of customized metal implants.[1] Although various types of CMPs have been designed for both animals[13,14] and human,[2,4,10–12] this approach has not yet been widely adopted and lacks complete follow-up results. The complex masticatory environment within the oral cavity may contribute to the failure of the operation. Therefore, factors such as structural rigidity and the design of a pressure-reducing device (PRD) should be considered to ensure the long-term success of this approach.[1,10–12,15,16] Studies on human and animal models have performed finite element analysis (FEA); an animal experiment was conducted to test the design[17] and the authors have applied for a patent for their PRD design (patent no: US 11,337,816 B2).

After lower-jaw reconstruction, patients often undergo denture reconstruction. A fibula flap is commonly selected because of its unique anatomical characteristics, which enable the precise segmentation and design of the fibula.[1,2,4] Many studies have focused on different fibula alignments and designs for subsequent implant surgery.[18,19] Jackson et al. reported that the overall implant survival rate was 93% and that the overall success rate of implant-supported prosthesis was 98% at a mean follow-up of 22 months. However, patients required the second stage of surgery after osseointegration between the implant fixture and fibular bone.[6]

Although sporadic case reports of 3D printed mandibles with incorporated dental implants have been published, no study has evaluated the structural design parameters of these implants.[5,20–22] Moreover, the dental implants on the CMP were usually structurally connected to the CMP, causing direct stress conduction. To improve the efficiency of stress dispersion during mastication, studies should consider exploring the use of implant PRD (iPRD) design in addition to the PRD of the CMP itself; this concept has not yet been explored in the literature.

FEA is used to simulate the mechanical aspect of a structure under load and has been widely used to predict the effect of stress on biomaterials and their surrounding structures.[8,23,24] The response surface methodology (RSM) involves a series of mathematical or statistical techniques for building empirical models and exploiting them. The RSM is used to determine the relationship between a response and the levels of input variables or factors that affect it. Compared with traditional formulation development approaches, the RSM is more efficient and cost effective, requiring less testing and time.[25,26] This study used the FEA method to conduct stress tests on the iPRD of the abutment and the RSM to determine the suitable structural assignment for the iPRD.

Materials and methods

Generation of the geometric model

The study protocol was approved by the Commission for Human Studies at the Institutional Review Board of Kaohsiung Veterans General Hospital, Kaohsiung, Taiwan (VGHKS19-CT6-14). All experiments were performed in accordance with the principles of the Declaration of Helsinki. Written informed consent was obtained from all patients or their legal guardian(s) for information/image publication, and patients agreed to reveal their facial photos

for academic purposes. We created digital models of the mandible by using the computed tomography (CT) scan of one of our patients. The CT scan was performed using a Kodak 9000 3D CBCT machine (Carestream Health, Inc., Rochester, NY, U.S.) with a slice thickness of 76 μm. We performed a 3D reconstruction of the mandible by using Mimics software (version 18.0, Materialize in Leuven, Belgium).

The defect area was defined in the unilateral mandibular body between the first premolar and the second molar. The CMP was designed to consist of the main body and the front and rear wings for fixation to the remaining mandible. Fig. 1A illustrates the configuration of fixing screws, with the front and rear wings secured using 3 and 4 screws, respectively. The posterior region of the main body of the CMP consisted of 3—5 parallel hollowed-out structures with terminal hollow cylinders at each line, which acted as a stress breaker structure (Fig. 1B). The iPRD at the base of the abutment served as a stress breaker structure, with cone length (CL) structures (Fig. 1C—F). We divided our model into various subunits, namely the anterior and posterior mandibular cortical bone, bone marrow, retentive screws, abutment, ceramic crown, and CMP (Fig. 1G-N).

Establishment of the finite element model and mesh sensitivity analysis

In this study, we used ANSYS Workbench (Swanson Analysis Systems Co., Houston, TX, USA) for simulation. We designed 4 types of CMP: CMP, CMP with iPRD, CMP-PRD, and CMP-PRD with iPRD (Fig. 2). Subsequently, we imported the mandibular cortical bone, bone marrow, 4 CMP types, retention screws, abutment, and ceramic crown to ANSYS Workbench for simulation. We meshed these models by using quadratic formulation, second-order, full integration, tetrahedral structural solid elements. Table 1 lists the average values of the aspect ratio and skewness. Previously, we performed convergence studies and controlled for the variability of results to less than 5% for models with different element sizes. We applied bond-type connections to interfaces between retentive screws and the mandible and between the mandibular cortical bone and bone marrow and frictional-type connections (friction coefficient = 0.3)[27—29] to interfaces between the cortical bone and bone marrow of the mandible and its corresponding CMP, abutment to CMP, and ceramic crown to abutment. We characterized the anterior and posterior mandibular cortical bone, bone marrow, retentive screws, abutment, ceramic crown, and CMP to have linear elastic and isotropic properties and adopted all elastic modulus and Poisson's ratio values from the relevant literature (Table 2).[30] In author's study,[17] a biomechanical test was performed using a finite element model to perform a sensitivity analysis. A mesh size of 2.75 mm and a quadratic formulation were selected for the CMP, mandible, and ceramic crown. The finer components, such as the iPRD, abutment, and threaded hole for the abutment of the CMP, were modeled with a mesh size of 1.5 mm (2A-D).

Boundary conditions

As depicted in Fig. 2E, the top surfaces of 2 condyles were fully restrained to prevent the rigid-body displacement of the mandible (indicated by the purple patch). Displacement in the vertical direction of corresponding occlusal contacts was constrained over the left mandibular molar and right mandibular first premolar region (indicated by the yellow patch). In this study, we analyzed the vectors of major masticatory muscles while clenching in a human model. Because segmental mandibular resection was performed in this study, we selected a reduced biting force of 300 N in the vertical direction in the contralateral molar region and 150 N in the bilateral canine and incisal region.[31] The right masseter and medial pterygoid muscles were stripped of the angle of the mandible and transected. Thus, these 2 muscles were not considered in this study. Seven pairs of major masticatory muscles were examined, namely the superficial and deep masseter; anterior, middle, and posterior temporalis; lateral and medial pterygoid; and digastric muscles; we did not examine the right masseter and right medial pterygoid muscles. The calculated muscle vectors were applied in FEA for boundary condition setting (Table 3).

Using response surface methodology to determine the optimal design of the implant pressure-reducing device

We examined the effect of the structural adjustment of the iPRD on stress dispersion (Fig. 4). Our structural design, featuring 2 implants on the CMP, represents the right first molar (Number 1) and right second premolar molar (Number 2), as depicted in Fig. 1F. We developed 2 parameters for the iPRD: cone length (CL) in the upper part and spring pitch (SP) in the lower part. The length of the cone indicates the length of the entire implant, with a longer cone resulting in a less significant spring structure in the lower half. The SP represents the distance between the threads of the lower half of the spring structure. Because 2 teeth are involved, we considered 4 parameters: CL1, SP1, CL2, and SP2.

As presented in Table 5 and Fig. 4, we conducted convergence studies to determine the optimal element size and mesh density and selected a mesh size of 1.25 mm and a quadratic formulation for our study (Fig. 4A). We fixed the screw holes of the front and rear wings in our FEA model (Fig. 4B) and applied 2 vertical downward stresses of 300 N on the top surface of the 2 implants. In the DesignXplorer environment, we generated samples by using the Latin hypercube sampling method, which effectively prevents repetitive sampling and requires 20%—40% fewer simulation loops than does the direct Monte Carlo simulation technique.[32,33] We analyzed 25 samples to examine response surface construction (Table 5).

Statistical analysis

We used the bivariate logistic regression test to examine associations between the 4 parameters (CL1, SP1, CL2, and SP2) of the iPRD and the maximum values of von Mises equivalent stress, total deformation, and safety factor determined using the RSM. All data analyses were performed using SPSS version 20.0 for Windows. All results are

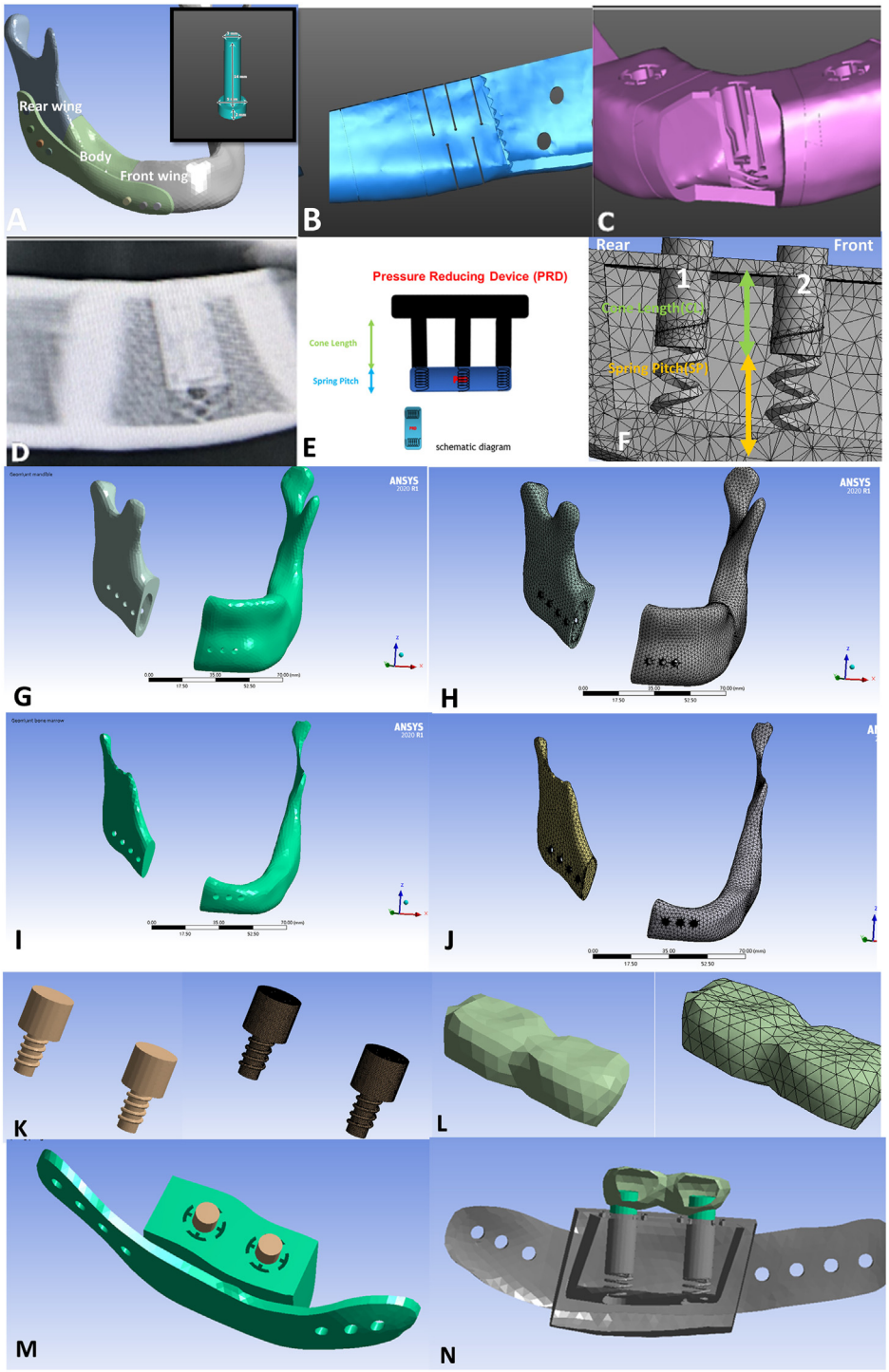

Figure 1 Structure of PRD and iPRD. (A) The CMP includes the main body, a front wing, and a rear wing and was fixed to the remaining mandible. The front wing was affixed with 3 screws, and the rear wing was affixed with 4 screws. (B)The PRD contains 3 to 5 parallel hollowed-out structures with terminal hollow cylinders at each line, which act as a stress breaker structure. (C) Interior view after surface removal. (D) Perspective view of the CMP through the panoramic film. (E, F) Structure design of the iPRD: The structure is mainly composed of the cone in the upper region and the spring in the lower region, and cone length and spring pitch are examined. (G, H) Mandibular cortical bone. (I, J) Mandibular bone marrow. (K) Abutments. (L) Ceramic crown. (M) CMP with abutment. (N) Perspective view of the CMP with iPRD, abutments, and ceramic crown. Abbreviations: CMP, customized mandible prostheses, PRD, pressure-reducing device, iPRD, implant pressure-reducing device, CL, cone length, SP, spring pitch.

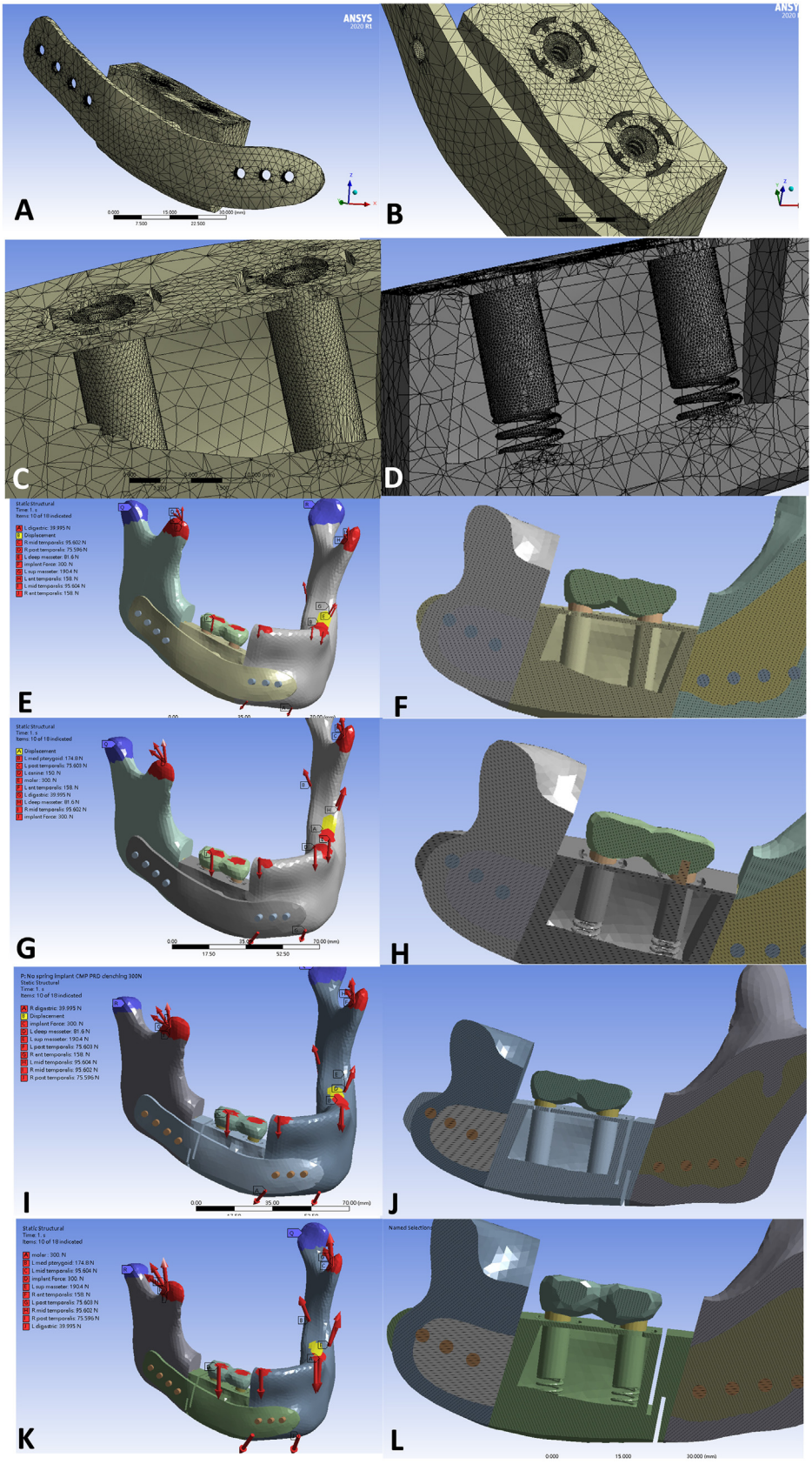

Figure 2 Structure of PRD and iPRD. (A) Lateral view of CMP. (B) Top view of CMP with screw holes for abutment insertion. (C) Perspective view of CMP. (D) Perspective view of CMP with iPRD. Calculated muscle vectors based on the results of 3D simulation in 4 types of CMP: CMP (E, F), CMP with iPRD (G, H), CMP-PRD (I, J), and CMP-PRD with iPRD (K, L). Abbreviations: CMP, customized mandible prostheses, PRD, pressure-reducing device, iPRD, implant pressure-reducing device.

Table 1 Number of nodes and elements and the average value of the aspect ratio and Skewness in 4 models. Abbreviations: CMP, customized mandible prothesis, PRD, pressure-reducing device, iPRD, implant pressure-reducing device.

	CMP	CMP + iPRD	CMP-PRD	CMP-PRD + iPRD
Mesh Nodes	738,595	782,901	771,663	818,928
Mesh Elements	421,275	445,657	440,546	466,707
Aspect ratio (average)	2.4998	2.4817	2.5115	2.4968
Skewness (average)	0.44667	0.44301	0.44817	0.44441

Table 2 Material properties of different components in the finite element model. Abbreviations: CMP, customized mandible prothesis, PRD, pressure-reducing device.

Type of material	Young's modulus [MPa]	Poisson's ratio
Mandible (cortex)	8700	0.28
Mandible (bone marrow)	1370	0.3
Ti6Al4 V (CMP, PRD and abutment)	105,000	0.3
Ti6Al4 V (screws)	105,000	0.3
Ceramic crown	108,000	0.33

Table 3 Total forces, stretched muscle weight, and calculated forces in X, Y, and Z directions during clenching in a human model. Abbreviations: sup., superficial, ant., anterior, mid., middle, post., posterior, lat., lateral. ant.

	Stretched Muscle Weight (N)	Unit Vector Coordinates		
		x	y	z
L sup. masseter	190.40	32.68	−93.65	201.61
L deep masseter	81.60	25.23	−13.49	87.17
R ant. temporalis	158.00	−10.63	4.58	169.55
R mid. temporalis	95.60	−28.83	44.52	103.04
R post. temporalis	75.60	−23.88	62.60	81.64
L ant. temporalis	158.00	−3.19	6.76	169.66
L mid. temporalis	95.60	18.10	48.97	103.18
L post. temporalis	75.60	14.29	65.11	81.71
L med. pterygoid	174.80	−83.94	−60.27	185.81
R lat. pterygoid	66.90	46.58	−32.02	68.71
L lat. pterygoid	66.90	−44.59	−35.91	68.59
R digastric	40.00	−2.55	31.29	43.00
L digastric	40.00	6.46	30.89	43.01
43-13	150.00	19.24	46.18	−141.41
33-23	150.00	−23.62	−33.06	−144.39
36-26	150.00	−23.27	23.27	−298.19
Loading to crowns	300.00	10.16	52.49	−295.2

presented as 2-tailed *P* values, and a *P* value of $< .05$ was considered statistically significant.

Results

Maximum von mises equivalent stress, principal stress, total deformation, and von mises equivalent strain in 4 forms of printed mandible prostheses

As presented in Table 4 and Fig. 3A, among the 4 forms of the CMP, CMP-PRD had the highest von Mises stress value for the entire assembly, followed by CMP-PRD with iPRD, CMP with iPRD, and CMP (1076.26, 1046.10, 575.56, and 482.04 MPa, respectively). For retentive screws, the CMP with iPRD had the highest von Mises stress value, followed by CMP, CMP-PRD, and CMP-PRD with iPRD (319.97, 318.97, 288.67, and 284.80 MPa, respectively). The structure of the PRD effectively reduced retentive screw stress, but the iPRD did not exert a prominent effect. For abutments, the CMP with iPRD had the highest von Mises stress value, followed by CMP-PRD with iPRD, CMP, and CMP-PRD (452.78, 413.24, 383.80, and 375.38 MPa, respectively). The structure of the iPRD, but not of the PRD, was effective in reducing abutment stress (Fig. 3C).

In the case of the anterior mandible, CMP-PRD had the highest principal stress value, followed by CMP-PRD with iPRD, CMP, and CMP with iPRD (131.66, 131.65, 124.91, and

Table 4 Maximum values of von Mises equivalent stress (entire assembly, CMP, retentive screws, and abutments), von Mises equivalent principal stress (anterior and posterior mandible), strain energy, total deformation, and von Mises equivalent strain in the 4 types of CMP. Abbreviations: CMP, customized mandible prothesis, PRD, pressure-reducing device, iPRD, implant pressure-reducing device.

	CMP	CMP with iPRD	CMP-PRD	CMP-PRD with iPRD	unit
Equivalent Stress-whole components and CMP	482.0446	575.5616	1076.2649	1046.0996	MPa
Equivalent Stress-screws	318.9664	319.9686	288.6659	284.7959	MPa
Equivalent Stress-abutments	383.8082	452.7751	375.3829	413.2440	MPa
Equivalent Principal Stress-ant mandible	124.9173	124.8055	131.6557	131.6501	MPa
Equivalent Principal Stress-post mandible	58.9285	57.4606	48.1237	48.0710	MPa
Strain Energy	0.5238	0.5234	0.5571	0.5572	mJ
Total Deformation	0.5593	0.5593	0.6087	0.6086	mm
Equivalent Elastic Strain	0.0123	0.0134	0.0144	0.0144	mm mm^-1

Table 5 Convergence studies were conducted to determine the optima element size and mesh density. Abbreviations: ant., anterior, post., posterior. % refers to the proportion of change in the measured value when convergence proceeds.

Mesh Element Size(mm)	Mesh Nodes	Mesh Elements	Equivalent Stress Maximum (MPa)		Equivalent Stress Maximum (MPa)-ant holes		Equivalent Stress Maximum (MPa) - post holes		Total Deformation Maximum (mm)	
2.5	24,375	13,007	105.16	%	94.003	%	99.72	%	0.0264	%
2	39,681	21,899	135.33	28.6896	103.8	10.4220	135.33	35.7100	0.0274	4.0408
1.75	59,317	33,023	102.82	−24.0228	95.305	−8.1840	102.82	−24.0228	0.0268	−2.1553
1.5	65,356	36,527	137.48	33.7094	137.48	44.2527	132.98	29.3328	0.0275	2.5307
1.25	69,753	38,813	146.93	6.8737	97.293	−29.2312	106.91	−19.6045	0.0275	−0.0073
1	90,989	51,388	140.08	−4.6621	104.02	6.9142	107.73	0.7670	0.0276	0.4762
0.75	131,792	131,792	157.55	12.4714	96.404	−7.3217	107.91	0.1671	0.0277	0.2750
0.5	233,355	173,577	136.82	−13.1577	114.27	18.5324	106.36	−1.4364	0.0278	0.3680

124.81 MPa, respectively). In the case of the posterior mandible, CMP had the maximum principal stress value, followed by CMP with iPRD, CMP-PRD, and CMP-PRD with iPRD (58.93, 57.46, 48.12, and 48.07 Mpa, respectively). Because the PRD is located at the posterior section of the CMP body, it might more effectively disperse stress in the posterior mandible and transfer stress to the anterior mandible, which has a stronger bone structure than the posterior mandible. Regardless of the presence of PRP, iPRD reduced principal stress in both the anterior and posterior mandible, although the degree of reduction was low (Table 4 and Fig. 3D).

Analysis of response surfaces

Fig. 4C and D displays the distribution of von Mises equivalent stress and displacement in the CMP with iPRD. Table 6 presents the data of 25 groups that were tested to obtain various results, including the maximum level of von Mises equivalent stress in the anterior and posterior screw holes, maximum level of total deformation, and safety factor of the CMP with iPRD under different changes in 4 parameters (CL1, SP1, CL2, and SP2). All the results in this study were automatically generated using the Ansys Workbench DesignXplorer program (Figs. 5 and 6). As CL1 increased, the maximum level of von Mises equivalent stress in the CMP with iPRD and anterior screw hole increased significantly ($r = .596$, $P = .002$ and $r = 0.578$, $P = .002$, respectively; Table 7). In this study, as CL1 increased, the safety factor decreased significantly ($r = -0.596$, $P = .002$). By contrast, as CL2 increased, the total deformation of the CMP with iPRD decreased ($r = -0.471$, $P = .018$). The optimal iPRD parameters are listed in Table 7. On the basis of our study results and for ease of 3D printing after numerous discussions with engineers specializing in 3D printing, we might set the CL to 12 mm and the SP to 0.4 mm for the subsequent clinical trials.

Discussion

Our FEA results revealed that the PRD deployed at the posterior region of the CMP transferred stress from the relatively fragile posterior mandible to the stronger anterior mandible in terms of the entire assembly. Our previous fracture test revealed that persistent stress can cause greenstick fractures on the lingual side of the posterior mandible (189 N).[17] Therefore, the transfer of stress from the posterior to the anterior mandible may be beneficial. We determined a reduction in the maximum stress on the retentive screw, which, in turn, reduced the likelihood of the screw breaking or falling off. Although the iPRD reduces stress on the anterior and posterior mandible simultaneously, these forces will concentrate upward on the abutment (375.38–452.78 MPa). The stress concentrated on abutments does not exceed the maximum yield strength

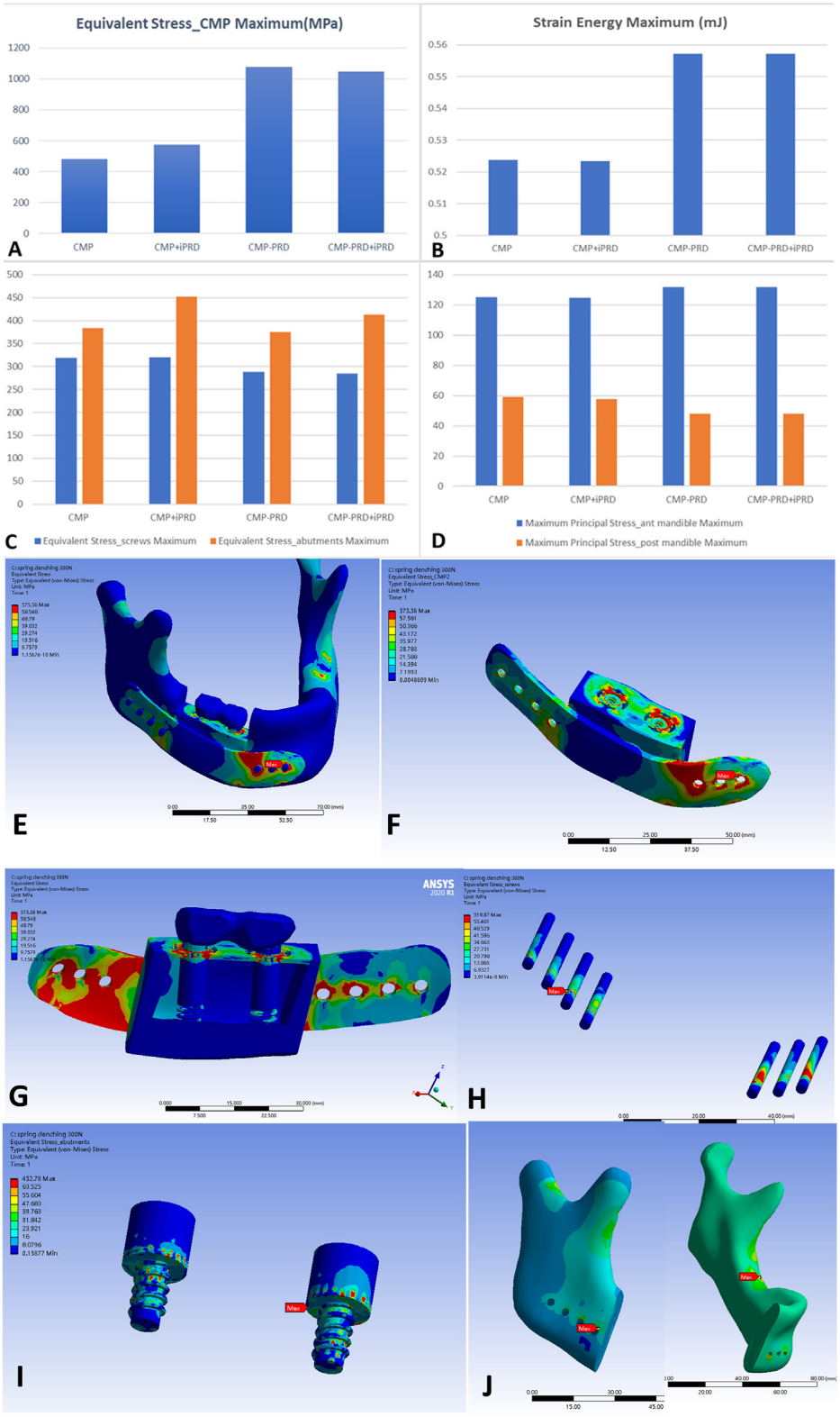

Figure 3 The maximum values of von Mises equivalent stress, strain energy, and von Mises equivalent principal stress in the 4 types of CMP. (A) Von Mises equivalent stress of the entire assembly. (B) Strain energy of the entire assembly. (C) Von Mises equivalent stress of retentive screws and abutments. (D) Von Mises principal stress of the anterior and posterior mandible. Von Mises equivalent stress of the entire assembly (E), CMP with iPRD (F), perspective view of CMP with iPRD (G), retentive screws (H), abutments (I), and anterior and posterior mandible (J). Abbreviations: CMP, customized mandible prostheses, PRD, pressure-reducing device, iPRD, implant pressure-reducing device.

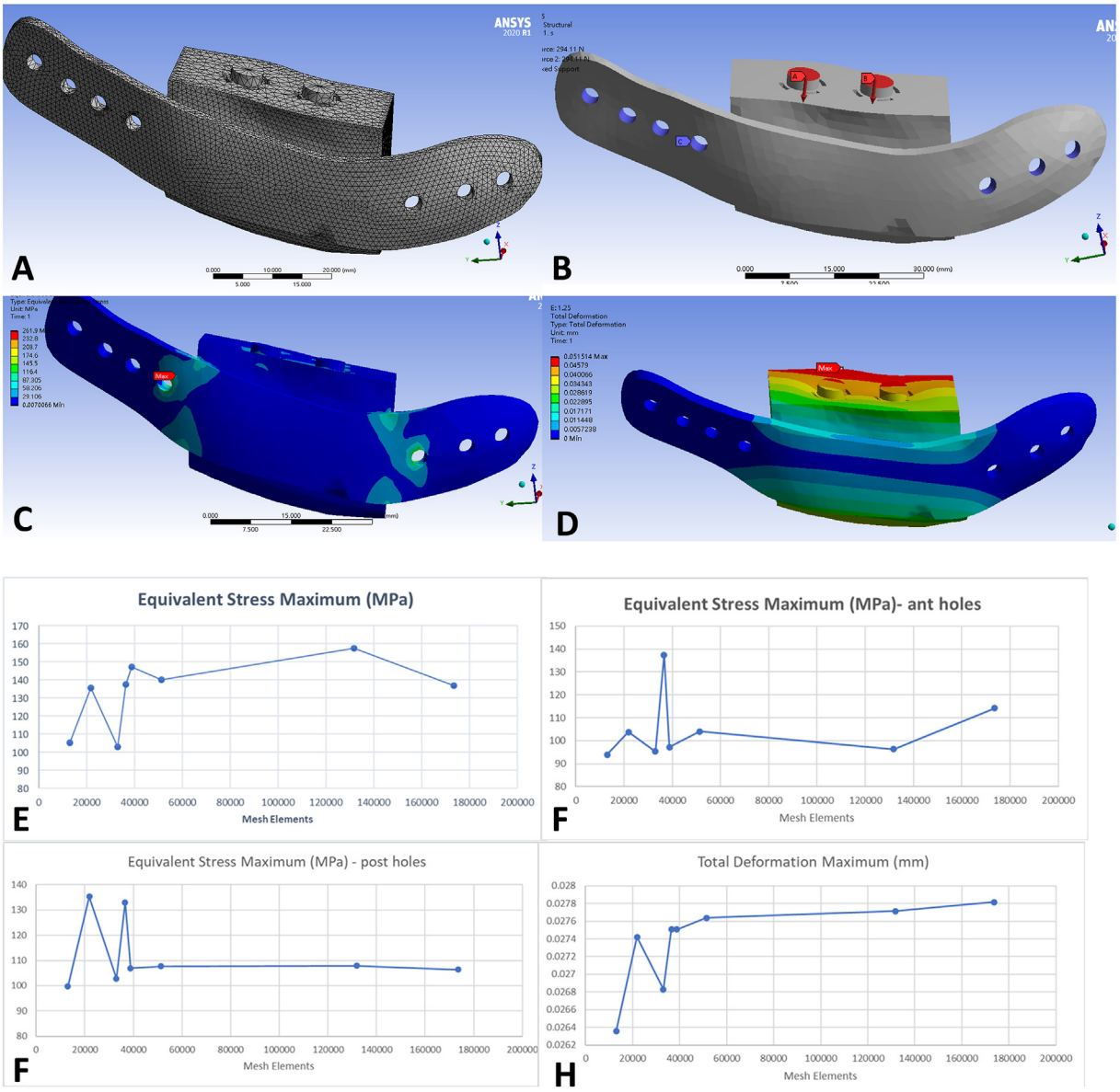

Figure 4 The response surface methodology (RSM) model. (A) A mesh size of 1.25 mm and a quadratic formulation were selected. (B) The screw holes of the front and rear wings were fixed and two vertical downward stress of 300 N on the top surface of the 2 implants were applied. (C) Von Mises equivalent stress of CMP with iPRD. (D) Total deformation of CMP with iPRD (E—H) Convergence studies were conducted to determine the optimal element size and mesh density. Abbreviations: CMP, customized mandible prostheses, PRD, pressure-reducing device, iPRD, implant pressure-reducing device.

of titanium itself (880—920 MPa).[34] The optimum iPRD parameters are listed in Table 6. On the basis of our study results and for ease of 3D printing, we might set the CL at 12 mm and the SP at 0.4 mm in the clinical trials.

Our simulations have some limitations that should be addressed in subsequent studies. In this study, we assumed bone material properties to be linear and isotropic. However, actual bone material is characterized as being anisotropic and inhomogeneous. The scholars[35,36] proposed using Hounsfield units from CT as a representation of a heterogeneous state, and to derive more groups based on this value in one sample. Therefore, to produce results that better align with the real clinical situation, these conditions should be considered in future studies. In our study, we used the maximum principal stress criteria in bone stress analysis. However, other studies have used different criteria to predict the failure of bone, such as the Hills criterion (an extension of the von Mises criterion) for the cortical bone[37] and the Tsai-Wu criterion (originally formulated for composite materials) to predict the multiaxial failure of the trabecular bone.[38] Incorporating these properties and criteria in subsequent studies can enhance the realism of our models.

Some sporadic case reports focus on the use of 3D printed mandibles with incorporated dental implants.[4,9,10,39,40] In these cases, the abutment was directly fused with the CMP. However, the concept of designing the iPRD based on masticatory stress dispersion efficiency remains unexplored.

Table 6 A total of 25 samples were analyzed for response surface construction and optimal iPRD parameters were obtained. Abbreviations: iPRD, implant pressure-reducing device, CL, cone length, SP, spring pitch.

Test Samples	CL1(mm)	SP1 (mm)	CL2 (mm)	SP2 (mm)	Equivalent Stress Maximum (MPa)	Equivalent Stress Maximum (MPa)-ant holes	Equivalent Stress Maximum (MPa) - post holes	Total Deformation Maximum (mm)	Safety Factor Minimum
1	16.0000	0.2750	16.0000	0.2750	101.7437	91.4839	101.7437	0.0267	4.5212
2	22.0000	0.2750	16.0000	0.2750	104.8620	90.6293	104.8620	0.0266	4.3867
3	10.0000	0.2750	16.0000	0.2750	104.2456	93.4082	104.2456	0.0267	4.4127
4	16.0000	0.1500	16.0000	0.2750	103.2738	91.6320	103.2738	0.0267	4.4542
5	16.0000	0.4000	16.0000	0.2750	101.7845	88.7263	101.7845	0.0267	4.5194
6	16.0000	0.2750	16.0000	0.1500	103.9720	90.2122	103.9720	0.0267	4.4243
7	16.0000	0.2750	16.0000	0.4000	103.1074	89.3698	103.1074	0.0267	4.4614
8	16.0000	0.2750	22.0000	0.2750	101.9277	89.2559	101.9277	0.0266	4.5130
9	16.0000	0.2750	10.0000	0.2750	101.2877	101.2877	99.7878	0.0256	4.5415
10	20.2252	0.1870	20.2252	0.1870	103.8883	91.9346	103.8883	0.0266	4.4278
11	11.7748	0.1870	20.2252	0.1870	103.2292	92.0956	103.2292	0.0266	4.4561
12	20.2252	0.3630	20.2252	0.1870	104.9779	91.9599	104.9779	0.0266	4.3819
13	11.7748	0.3630	20.2252	0.1870	99.3354	93.2647	99.3354	0.0266	4.6308
14	20.2252	0.1870	20.2252	0.3630	104.7704	92.9882	104.7704	0.0266	4.3906
15	11.7748	0.1870	20.2252	0.3630	103.1961	89.2959	103.1961	0.0265	4.4575
16	20.2252	0.3630	20.2252	0.3630	101.7958	93.7658	101.7958	0.0266	4.5189
17	11.7748	0.3630	20.2252	0.3630	101.1369	94.3784	101.1369	0.0266	4.5483
18	20.2252	0.1870	11.7748	0.1870	103.1708	88.3229	103.1708	0.0266	4.4586
19	11.7748	0.1870	11.7748	0.1870	101.0051	92.9815	101.0051	0.0268	4.5542
20	20.2252	0.3630	11.7748	0.1870	104.4395	92.2072	104.4395	0.0266	4.4045
21	11.7748	0.3630	11.7748	0.1870	100.1368	94.3169	100.1368	0.0267	4.5937
22	20.2252	0.1870	11.7748	0.3630	105.8918	91.6644	105.8918	0.0266	4.3441
23	11.7748	0.1870	11.7748	0.3630	98.8333	94.5354	98.8333	0.0267	4.6543
24	20.2252	0.3630	11.7748	0.3630	102.9328	92.5413	102.9328	0.0266	4.4689
25	11.7748	0.3630	11.7748	0.3630	99.1920	91.4501	99.1920	0.0267	4.6375
Option 1	11.1447	0.3939	21.2934	0.1573	98.6285	92.6871	97.5627	0.0265	4.6626
Option 2	12.1774	0.3998	12.2290	0.3998	99.5037	91.0756	98.7359	0.0268	4.6236
Option 3	12.2163	0.3995	13.5952	0.3998	99.9350	89.8687	99.7236	0.0269	4.6039

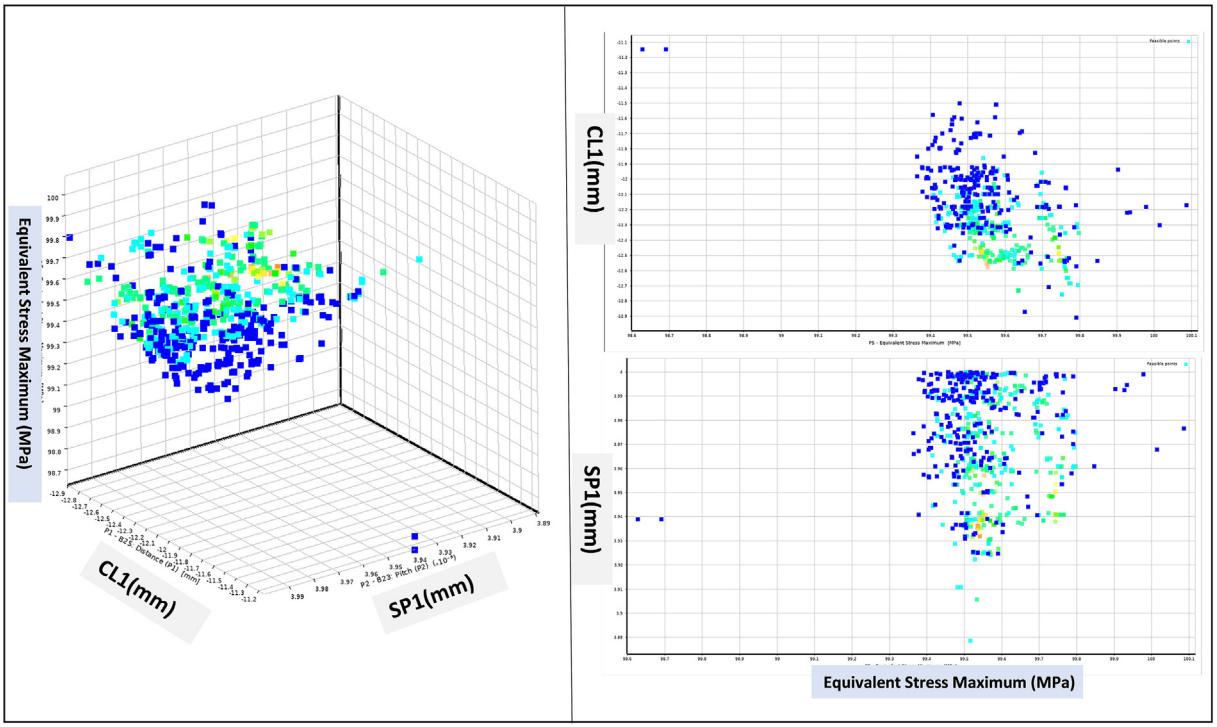

Figure 5 Response surfaces of CL1 and SP1 to von Mises equivalent stress in CMP with iPRD. Abbreviations: CMP, customized mandible prostheses, CL, cone length, SP, spring pitch.

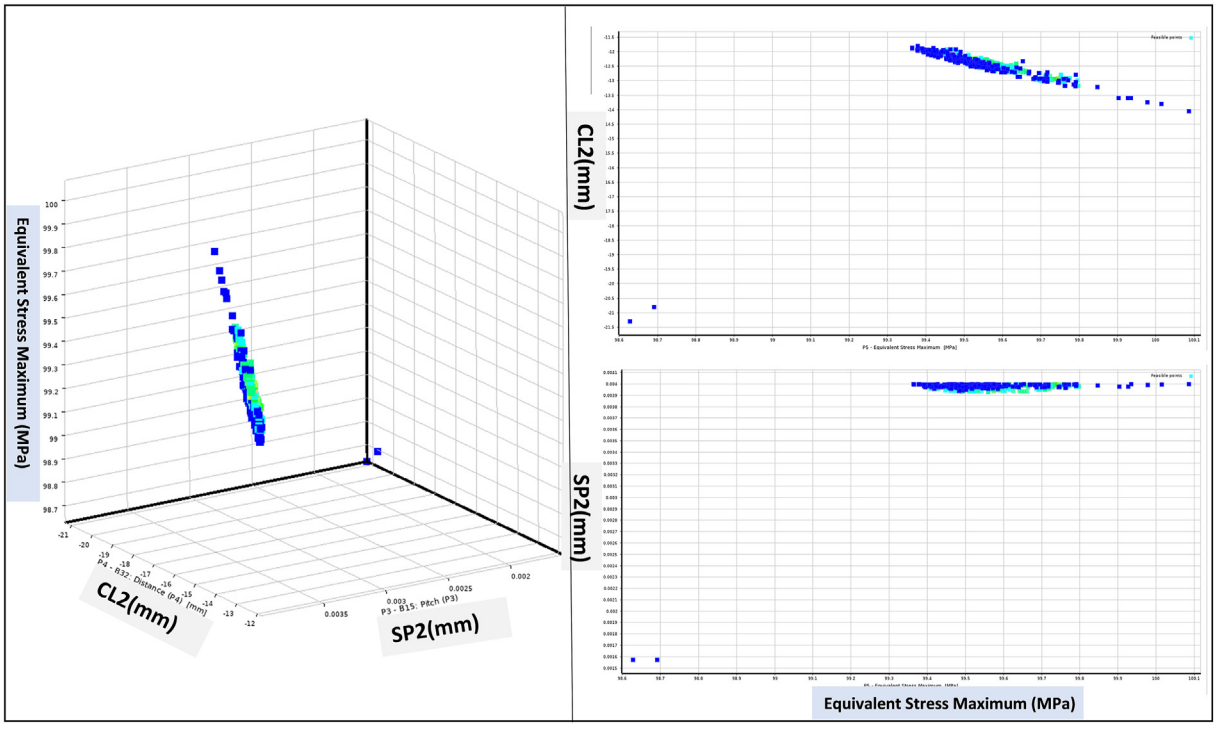

Figure 6 Response surfaces of CL2 and SP2 to von Mises equivalent stress in CMP with iPRD. Abbreviations: CMP, customized mandible prostheses, CL, cone length, SP, spring pitch.

Table 7 Spearman's rank correlation between the CL1, SP1, CL2, and SP2 and the maximum value of von Mises equivalent stress in anterior and posterior screw holes, CMP with iPRD, total deformation, and safety factor. Abbreviations: CMP, customized mandible prostheses, PRD, pressure-reducing device, iPRD, implant pressure-reducing device, CL, cone length, SP, spring pitch.

Spearman's Correlation		Equivalent Stress Maximum (MPa)	Equivalent Stress Maximum (MPa)-ant holes	Equivalent Stress Maximum (MPa) - post holes	Total Deformation Maximum (mm)	Safety Factor Minimum
CL1(mm)	r-value	**0.596**[b]	−0.27	**0.578**[b]	−0.13	**−0.596**[b]
	p-value	0.002	0.191	0.002	0.535	0.002
SP1 (mm)		−0.282	0.14	−0.276	−0.029	0.282
		0.171	0.504	0.181	0.891	0.171
CL2 (mm)		0.22	−0.152	0.243	**−0.471**[a]	−0.22
		0.291	0.468	0.243	0.018	0.291
SP2 (mm)		−0.13	0.063	−0.136	0.034	0.13
		0.535	0.766	0.516	0.873	0.535

[a] Correlation is significant at the .05 level (2-tailed) r = Spearman's rank correlation coefficient.
[b] Correlation is significant at the .01 level (2-tailed).

Although various types of CMP have been developed, their widespread use is still limited. In this study, we designed a CMP with incorporated dental implants and explored the use of an iPRD. FEA results revealed that the PRD deployed at the posterior portion of the CMP transferred stress from the relatively fragile posterior mandible to the stronger anterior mandible. The iPRD reduced principal stress in both the anterior and posterior mandible. We need further clinical trials to verify our results.

Declaration of competing interest

The authors declare no conflicts of interest in relation to this study.

Acknowledgment

This study was supported by grants from Kaohsiung Veterans General Hospital (KSVGH110-099) and Southern Taiwan Science Park (STSP) (Grant: BX-03-04-04-110).

References

1. Szabo G, Barabas J, Bogdan S, Nemeth Z, Sebok B, Kiss G. Long-term clinical and experimental/surface analytical studies of carbon/carbon Maxillofacial Implants. *Maxillofac Plast Reconstr Surg* 2015;37:34.
2. Rachmiel A, Shilo D, Blanc O, Emodi O. Reconstruction of complex mandibular defects using integrated dental custom-made titanium implants. *Br J Oral Maxillofac Surg* 2017;55:425—7.
3. Cordeiro PG, Disa JJ, Hidalgo DA, Hu QY. Reconstruction of the mandible with osseous free flaps: a 10-year experience with 150 consecutive patients. *Plast Reconstr Surg* 1999;104:1314—20.
4. Jo YY, Kim SG, Kim MK, Shin SH, Ahn J, Seok H. Mandibular reconstruction using a customized three-dimensional titanium implant applied on the lingual surface of the mandible. *J Craniofac Surg* 2018;29:415—9.
5. Goh BT, Lee S, Tideman H, Stoelinga PJ. Mandibular reconstruction in adults: a review. *Int J Oral Maxillofac Surg* 2008;37:597—605.
6. Kim JW, Hwang JH, Ahn KM. Fibular flap for mandible reconstruction in osteoradionecrosis of the jaw: selection criteria of fibula flap. *Maxillofac Plast Reconstr Surg* 2016;38:46.
7. Brown JS, Barry C, Ho M, Shaw RA. New classification for mandibular defects after oncological resection. *Lancet Oncol* 2016;17:e23—30.
8. Wilde F, Hanken H, Probst F, Schramm A, Heiland M, Cornelius CP. Multicenter study on the use of patient-specific cad/cam reconstruction plates for mandibular reconstruction. *Int J Comput Assist Radiol Surg* 2015;10:2035—51.
9. Toure G, Gouet E. Use of a 3-dimensional custom-made porous titanium prosthesis for mandibular body reconstruction with prosthetic dental rehabilitation and lipofilling. *J Oral Maxillofac Surg* 2019;77:1305—13.
10. Lee YW, You HJ, Jung JA, Kim DW. Mandibular reconstruction using customized three-dimensional titanium implant. *Arch Craniofac Surg* 2018;19:152—6.
11. U V, Mehrotra D, Howlader D, Singh PK, Gupta S. Patient specific three-dimensional implant for reconstruction of complex mandibular defect. *J Craniofac Surg* 2019;30:e308—11.
12. Dahake S, Kuthe A, Kulkarni S, Mawale M. Finite element analysis of customized implant in mandibular reconstruction after tumor resection with and without using customized surgical osteotomy guide. *Int J Med Robot* 2018;14:e1854.
13. Lee SW, Kim HG, Ham MJ, Hong DGK, Kim SG, Rotaru H. Custom implant for reconstruction of mandibular continuity defect. *J Oral Maxillofac Surg* 2018;76:1370—6.
14. Markwardt J, Sembdner P, Lesche R, et al. Experimental findings on customized mandibular implants in gottingen minipigs - a pilot study. *Int J Surg* 2014;12:60—6.
15. Cheng KJ, Liu YF, Wang R, et al. Topological optimization of 3d printed bone analog with pekk for surgical mandibular reconstruction. *J Mech Behav Biomed Mater* 2020;107:103758.
16. Langenbach GE, Zhang F, Herring SW, Hannam AG. Modelling the masticatory biomechanics of a pig. *J Anat* 2002;201:383—93.
17. Chen CF, Chen CM, Chen HS, et al. The use of customized three-dimensionally printed mandible prostheses with a pressure-reducing device: a finite element analysis in different chewing positions, biomechanical testing, and in vivo animal Study Using Lanyu Pigs. *BioMed Res Int* 2022;2022:9880454.
18. Yu Y, Zhang WB, Liu XJ, Guo CB, Yu GY, Peng X. Three-dimensional accuracy of virtual planning and surgical navigation for mandibular reconstruction with free fibula flap. *J Oral Maxillofac Surg* 2016;74:1503 e1—e03 e10.

19. Okoturo E. Non-vascularised iliac crest bone graft for immediate reconstruction of lateral mandibular Defect. *Oral Maxillofac Surg* 2016;20:425—9.
20. Cohen A, Laviv A, Berman P, Nashef R, Abu-Tair J. Mandibular reconstruction using stereolithographic 3-dimensional printing modeling technology. *Oral Surg Oral Med Oral Pathol Oral Radiol Endod* 2009;108:661—6.
21. Shibahara T, Noma H, Furuya Y, Takaki R. Fracture of mandibular reconstruction plates used after tumor resection. *J Oral Maxillofac Surg* 2002;60:182—5.
22. Lopez R, Dekeister C, Sleiman Z, Paoli JR. Mandibular reconstruction using the titanium functionally dynamic bridging plate system: a retrospective study of 34 cases. *J Oral Maxillofac Surg* 2004;62:421—6.
23. Ciocca L, Fantini M, De Crescenzio F, Corinaldesi G, Scotti R. CAD-CAM prosthetically guided bone regeneration using preformed titanium mesh for the reconstruction of atrophic maxillary arches. *Comput Methods Biomech Biomed Eng* 2013;16:26—32.
24. Tarsitano A, Del Corso G, Ciocca L, Scotti R, Marchetti C. Mandibular reconstructions using computer-aided design/-computer-aided manufacturing: a systematic review of a defect-based reconstructive algorithm. *J Cranio-Maxillo-Fac Surg* 2015;43:1785—91.
25. Probst FA, Metzger M, Ehrenfeld M, Cornelius CP. Computer-assisted designed and manufactured procedures facilitate the lingual application of mandible reconstruction plates. *J Oral Maxillofac Surg* 2016;74:1879—95.
26. Hong KDG, Kim SG, Park YW. The effect of fixation plate use on bone healing during the reconstruction of mandibular defects. *J Korean Assoc Oral Maxillofac Surg* 2019;45:276—84.
27. Braic V, Balaceanu M, Braic M, Vladescu A, Panseri S, Russo A. Characterization of multi-principal-element (tizrnbhfta)n and (tizrnbhfta)c coatings for biomedical applications. *J Mech Behav Biomed Mater* 2012;10:197—205.
28. Xu Y, Liu W, Zhang G, et al. Friction stability and cellular behaviors on laser textured ti-6al-4v alloy implants with bio-inspired micro-overlapping structures. *J Mech Behav Biomed Mater* 2020;109:103823.
29. Choudhury D, Lackner JM, Major L, et al. Improved wear resistance of functional diamond like carbon coated Ti-6al-4v alloys in an edge loading conditions. *J Mech Behav Biomed Mater* 2016;59:586—95.
30. Li P, Tang Y, Li J, Shen L, Tian W, Tang W. Establishment of sequential software processing for a biomechanical model of mandibular reconstruction with custom-made plate. *Comput Methods Progr Biomed* 2013;111:642—9.
31. Linsen SS, Oikonomou A, Martini M, Teschke M. Mandibular kinematics and maximum voluntary bite force following segmental resection of the mandible without or with reconstruction. *Clin Oral Invest* 2018;22:1707—16.
32. Monirul Islam M, Hemmanahalli Ramesh V, Durga Bhavani P, et al. Optimization of process parameters for fabrication of electrospun nanofibers containing neomycin sulfate and malva sylvestris extract for a better diabetic wound healing. *Drug Deliv* 2022;29:3370—83.
33. Sreeharsha N, Prasanthi S, Mahalakshmi S, et al. Enhancement of anti-tumoral properties of paclitaxel nano-crystals by conjugation of folic acid to pluronic F127: formulation optimization, in vitro and in vivo study. *Molecules* 2022;27:7914.
34. Long M, Rack HJ. Titanium alloys in total joint replacement–a materials science perspective. *Biomaterials* 1998;19:1621—39.
35. Aquilina P, Parr WC, Chamoli U, Wroe S. Finite element analysis of patient-specific condyle fracture plates: a preliminary study. *Craniomaxillofacial Trauma Reconstr* 2015;8:111—6.
36. Hijazi L, Hejazi W, Darwich MA, Darwich K. Finite element analysis of stress distribution on the mandible and condylar fracture osteosynthesis during various clenching tasks. *Oral Maxillofac Surg* 2016;20:359—67.
37. Sharma D, Ciani C, Marin PA, Levy JD, Doty SB, Fritton SP. Alterations in the osteocyte lacunar-canalicular microenvironment due to estrogen deficiency. *Bone* 2012;51:488—97.
38. Keaveny TM, Wachtel EF, Zadesky SP, Arramon YP. Application of the tsai-Wu quadratic multiaxial failure criterion to bovine trabecular bone. *J Biomech Eng* 1999;121:99—107.
39. Lim HK, Choi YJ, Choi WC, Song IS, Lee UL. Reconstruction of maxillofacial bone defects using patient-specific long-lasting titanium implants. *Sci Rep* 2022;12:7538.
40. Park JH, Odkhuu M, Cho S, Li J, Park BY, Kim JW. 3D-Printed titanium implant with pre-mounted dental implants for mandible reconstruction: a Case Report. *Maxillofac Plast Reconstr Surg* 2020;42:28.